IMPROVED EXPERIMENTAL TECHNIQUES FOR LIFE PREDICTION UNDER THERMOMECHANICAL FATIGUE (TMF) CONDITIONS

Aitor García de la Yedra, Antonio Martín-Meizoso, Jose Luis Pedrejón

CEIT and TECNUN (University of Navarra)

Paseo de Manuel Lardizábal, 15, 20018 San Sebastián, Spain

ABSTRACT

Turbine hot section materials, superalloys, are subjected to variable loads (pressure and centrifugal) as well as variable thermal loads due to start ups and shutdowns which yields to a thermomechanical fatigue (TMF) condition. Under these conditions it is known that three kinds of degradations lead the material to fracture: creep, fatigue and oxidation, but the interaction among them is not well understood. This is why experimental techniques play an important role.

The main objective is to obtain a test-machine configuration which fulfils the corresponding ASTM standard in terms of temperature distribution, alignment, thermal and mechanical strain control, etc. This paper is focused on the former field. For that purpose some measurements were carried out with thermocouples as well as an infrared thermopraphic camera. In some cases theoretical solutions were needed (analytical and finite element method solutions) due to the fact that repetitiveness was not achieved. As a result of the different actions a configuration was obtained which allows executing thermomechanical fatigue tests.

KEY WORDS*:* Thermomechanical fatigue; thermal gradients; Finite Element Method

1. INTRODUCTION

TMF tests are carried out to broaden knowledge on the degradation methods of materials which suffer thermal and mechanical cyclic loads. Therefore these tests involve mechanical strain as well as thermal strain cycles applied simultaneously. The former is obtained by using a servoelectric test machine (INSTRON 8562), whereas thermal strain cycles are accomplished taking advantage of the Joule effect, instead of the usual induction heating system. The main challenge in this field is to obtain a configuration in which thermal distribution is as homogeneous as possible. It is known that heterogeneous distributions cause thermally induced additional stresses. This magnitude and temperatures have been assessed using different available tools (analytical and numerical solutions as well as experimental measurements with thermocouples and IR thermographic camera). As a result of the former action, a configuration was obtained which allows reducing previous thermal gradients and fulfilling the corresponding ASTM standard [1].

2.TEMPERATURE DISTRIBUTION MEASUREMENTS

Firstly, some experiments were accomplished to pursue the understanding of the temperature distribution along the test machine axis (axial gradients) with no mechanical strain applied. Three ribbon thermocouples (TC, N type) were used, placed one in the centre of the gauge length (12.5 mm) and the other two at the end of it, as shown in Figure 1.

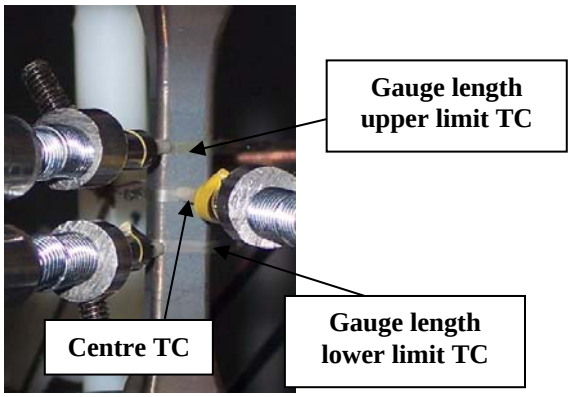

Figure 1. TC configuration

Thermal cycles range was 300ºC-950ºC with a 5ºC/s heating and cooling rates. Control temperature was carried out with central thermocouple. Test-pieces are of rectangular cross-section, 8 mm width and 5 mm thick, with corner radius of 1 mm. The material to test is stainless steel AISI 316. Although its mechanical properties differ from those of superalloys, its thermal properties turn out to be similar, if relative difference in thermal diffusivity is considered [2]. This magnitude gives an idea of the thermal inertia and the transient state, reaching the steady state more rapidly if the thermal diffusivity is higher.

Heating source (Q) is obtained thanks to the voltage drop (ΔV) when an electric current (I) passes through the test-piece.

$$Q = \Delta V\, I \quad (1)$$

At the same time, voltage drop is directly proportional to the electric resistance (R) which increases with the test-piece length (L) and decreases with its area (A).

$$\Delta V = I\, R \quad (2)$$

$$R = \rho\, L/A \quad (3)$$

This property and the test-piece geometry cause huge differences in heat source, yielding a situation where within the gauge length heat source is 50 % higher than at the ends of the test-piece. This may provoke high thermal gradients. For this reason another experiment was accomplished adding a heat source to the test machine grips by using 460 W electric resistances and surrounded by some alumina boxes as shown in Figure 2.

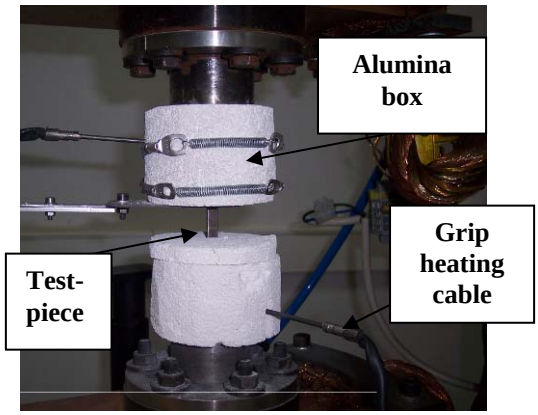

Figure 2. Grip heating method

This allowed heating those parts of the test piece where heating source was low. Besides the alumina boxes reduced heat losses, improving the efficiency of the method. The same three thermocouples, as in the previous experiments, were used placed in the same positions and some TMF thermal cycles were carried out.

Eventually, an infrared thermo graphic camera was used to contrast the results with the measurements accomplished with thermocouples due to the fact that repetitiveness in measurements was hard to achieve in some cases. As a non-contact temperature measurement method, the image obtained is a function of a material property (emissivity) which changes with temperature, surface roughness and oxidation. The strategy to avoid this drawback was to use a thermocouple at the centre of the gauge length and heat the test-piece up to the peak temperature of the TMF cycle (950ºC). If this temperature is maintained, after some time oxidation level reaches its maximum and this allows calibrating the camera with a constant emissivity value, typically 0,85. Afterwards, an image was obtained at that precise temperature for a steady state.

Measuring temperature with an IR thermography camera in a transient cycle involves a very good knowledge of emissivity value at different temperatures as well as at different oxidation states. This aspect is not covered in this paper.

Regarding radial temperature distribution, a 0.3 mm hole was drilled up to the core of one test-piece. The hole has to be small enough to not disturb the temperature distribution within the cross-section, but it also has to be large enough to fit a thermocouple (N type, Nicrosil-Nisil). However, handling of small diameter thermocouples turns out to be difficult and repetitiveness is not achieved. Some other authors have found the same difficulty when measuring radial gradients in a cross section [3]. This is why theoretical solutions were preferred.

3. THEORETICAL SOLUTIONS

3.1- Analytical solution

Heat transfer problems are governed by the following equation:

$$k\left(\frac{\delta^2 T}{\delta x^2}+\frac{\delta^2 T}{\delta y^2}+\frac{\delta^2 T}{\delta z^2}\right)+q=\rho\cdot c\cdot\frac{\delta T}{\delta t} \quad (4)$$

where k (W/m.K) is the thermal conductivity of the material, ρ (kg/m^3) the density, c (J/kg.K) specific heat, T (K) temperature and q (W/m^3) the heat source produced by the voltage drop described in equation (1).

If radial gradients are needed to assess, the partial differential equation, for a rectangular parallelepiped, may be solved assuming that no heat generation exists (TMF cooling cycle). It is also assumed that the initial temperature distribution is known and is considered homogeneous.

Equation (4) was solved using the superposition method and considering the following boundary conditions:

a) $-k\left(\frac{\delta T}{\delta x}\right)=h.[T(L,t)-T\infty]$, convection heat exchange of the outer surface on each main direction (x, y, z) ……... (5), where h=10 W/m^{2}K is the film coefficient.

b) $T(x, y, z, 0) = T_i$=1223K $\forall x, y, z$ initial homogeneous temperature distribution……(6)

Radiation effect, which is the most damaging in terms of radial gradients, may be taken into account in

equation (5) if an equivalent film coefficient is defined. The radiation heat exchange may be rewritten as follows:

$$Q_{radiation} = \sigma \cdot \varepsilon \cdot (T^4 - T_\infty^4) \quad (7)$$

$$Q_{radiation} = \sigma \varepsilon (T + T_\infty)(T^2 + T_\infty^2)(T - T_\infty) \quad (8)$$

where σ stands for the Stefan Boltzmann constant 5.67. 10^{-8} W/m^{2}K^4, ε for the emissivity value (no units) and T_∞ for the room temperature. Equation (8) may be written in the same manner to the convection heat exchange if a radiation film coefficient is introduced ($h_r[W/m^2 \cdot K^4]$):

$$Q_{radiation} = h_r (T - T_\infty) \quad (9)$$

$$h_r = \sigma \cdot \varepsilon \cdot (T + T_\infty) \cdot (T^2 + T_\infty^2) \quad (10)$$

The above mentioned consideration was taken into account and equation (4) was solved by using a Matlab 7.5 code and an equivalent film coefficient which is a sum of convection and radiation coefficients. It was solved with 0.1 second time increments and considering property changes with temperature on each one.

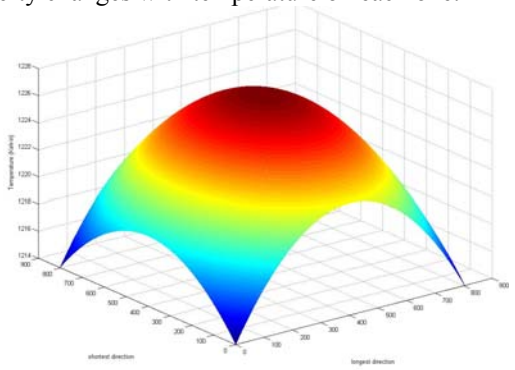

Figure 3. Analytical solution for radial gradients worst scenario in a TMF cycle

Figure 3 shows the initial and worst instant for the TMF cooling cycle. The obtained gradients were around 9ºC but after plotting the complete thermal transient a conclusion was drawn; achieved cooling rates were higher than 5ºC/s which is the value for a typical TMF test. This means that obtained thermal gradients are higher than in a real test where cooling rate is lower.

Figure 4 displays the thermal transient analysis for a two cross section spots: core, which gave the maximum temperature value and edge, which corresponds with the minimum. Besides, 5ºC/s cooling rate was plotted to compare it with the achieved curves.

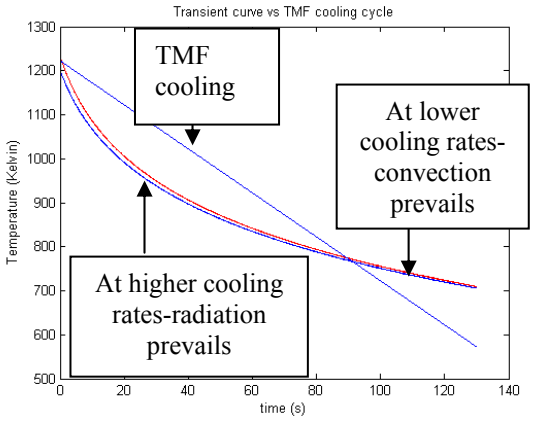

Figure 4. Transient TMF cycle for maximum (core) and minimum (edge) temperatures compared with 5ºC/s cooling rate

It was observed that if this cooling rate was needed to be followed, an input electrical current would have to pass through the test-piece during the first 90 seconds. On the other hand, when test-piece reached lower temperature values its cooling rate was very low and convection has to be forced to follow the desired ramp by blowing some cold air through some nozzles. This effect happens due to the radiation, which involves large heat exchange when temperatures are high, but it may be neglected if temperatures are sufficiently low.

Consequently, heat source due to the Joule effect should be added to equation (4) to obtain the desired ramp. Nevertheless, a coupling effect exists between Joule effect and thermal problem which makes the obtaining of the analytical transient response difficult. Therefore, numerical solutions are thought to be the best option to face the problem.

3.2- Numerical solutions

ABAQUS finite element method *(FEM)* software provides a coupled thermal-electric code suitable for solving problems such as the one introduced in this paper. Coupling arises when heat generation has to be calculated. Firstly the electrical problem has to be solved but the electric conductivity and the input current are temperature dependent. This means that they can not be known before assessing the heat source. This involves an iterative process which is solved using numerical tools.

The model simulated by FEM consists of an eight of the test-piece, due to symmetry, and the following loads and boundary conditions:

a) Input electrical current
b) 0 electric potential at the end of the test-piece.
c) Convection and radiation heat exchange with the surrounding.
d) Adiabatic surfaces, at the three planes of symmetry.

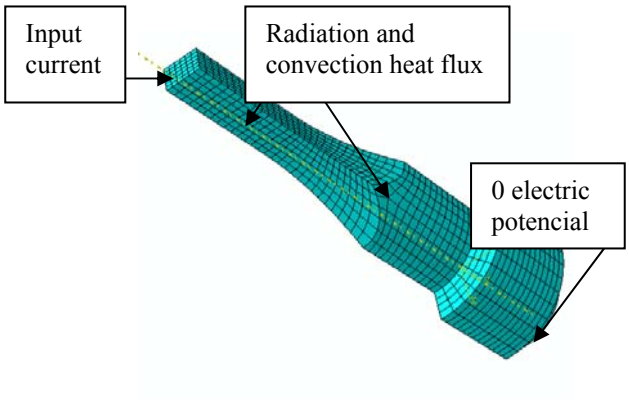

Figure 5. FEM model for the coupled thermal-electric problem

Input electrical current was measured experimentally and recorded as a function of time for a typical TMF cycle. This allows reproducing a complete transient cycle. There are some electrical and thermal properties that change with temperature and their values are needed if accuracy in the results is desired. To achieve this purpose, experimentally the test-piece was heated up to three different temperature values (350ºC, 650ºC and 950 ºC measured at the centre of the gauge length).These temperatures were maintained and the input currents were measured. Afterwards, steady state FEM analyses were carried out, for each case, trying to match theoretical results with the ones obtained experimentally by changing the thermal and electrical properties. Three were the main properties to change, thermal and electrical conductivity as well as the emissivity. The former is obtained from the data available in the bibliography [2], this means that this value change with temperature is known and therefore it was fixed in the simulations .The rest of the properties values were modified until a matching between experimental and theoretical results was obtained. As a result of the experiments the following properties were obtained for the AISI 316 stainless steel.

Table 1. AISI 316 thermal and electrical properties as a function of temperature

Temperature reached in simulations(ºC)	Thermal conductivity (W/m·K)	Electric resistivity (Ohm·m)	Emissivity
355,05	18	7,00E-07	0,7
655,25	25	8,00E-07	0,8
950,85	28	9,00E-07	0,85

Regarding convection, in the tested range, radiation heat exchange prevails over convection, as it was proved with the analytical solutions, and therefore its influence in the heat phenomena is low, unless convection is forced. However, its effect was added to the simulation with a film coefficient *(h)* equal to 10 [W/m^2.K] constant throughout the cycle, which is a typical value for natural convection.

The correct execution of the simulation generates a file with the temperature distribution for the geometry drawn and at any instant of the complete TMF cycle modelled. This file was used to carry out a static analysis to assess the induced stresses due to heterogeneous temperature distribution.

4. RESULTS

4.1 Experimental results

The results of the experiments showed that, unless further actions are taken, axial thermal gradients will exist (up to 25ºC when peak temperature is reached). It has to be noted that the corresponding standard [1] limits this value to 1% of the peak absolute temperature (Kelvin), in other words to 12.23 ºC.

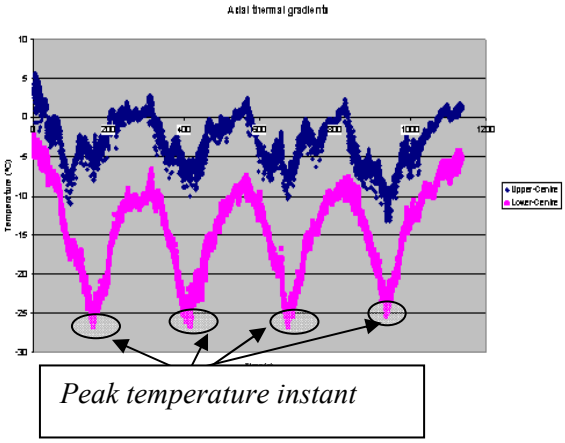

Figure 6. TMF axial gradients results for four cycles

In Figure 6 temperature measurements at the ends of the gauge length are displayed and compared to the centre thermocouple for four TMF cycles. According to the results maximum gradients happen when TMF cycle reaches its maximum temperature value, being centre thermocouple measurement much higher than those at the ends of the gauge length. It also has to be noted that the temperature at the lower gauge length limit (pink line, Figure 6) is much cooler than that at the upper gauge length limit (blue line, Figure 6) which may be attributed to the mass diffusivity effect. This means that hot air (with lower density) tends to ascend and this causes higher temperatures.

IR thermography method verifies that, even in a steady state case, axial gradients appear. Besides it helps to understand why those thermal differences occur, concluding that heat source at the end of the test-piece is low. This causes large heat flux due to conduction. An image (Figure 7) taken from that experiment clarifies what is explained here.

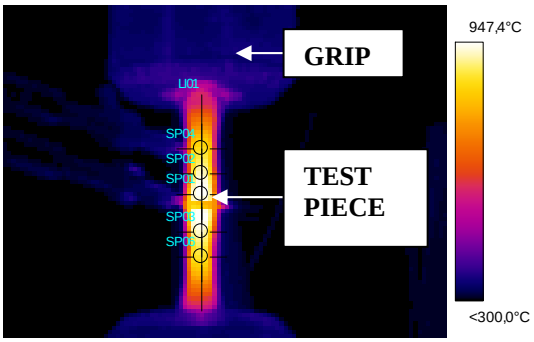

Figure 7. IR thermographic image (950ºC at the centre of the gauge length)

Figure 7 represents an instant of the test-piece and its grips when control thermocouple (centre) displays 950 ºC. Five points temperature were assessed, one placed in the centre, two close to the gauge length limit and the other two out of the gauge length. These measurements proved that within the gauge length temperature differences were around 25ºC, similar to those obtained by thermocouples, whereas those placed outside displayed differences above 100ºC. This confirms that heat flux from test-piece towards grips is huge, because of the temperature differences between them (950ºC at the former and only 300ºC at the grips).

Latest experiments (see Figure 2) with 460 W resistances for heat supplying to the grips gave excellent results as shown in ***Figure 8***:

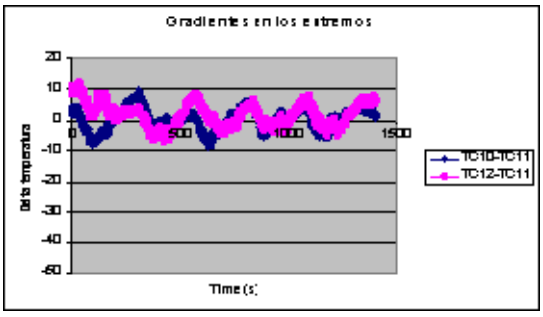

Figure 8. TMF axial gradients with grip preheating method

According to the latest results, current thermal cycles fulfil the corresponding standard [1] as they do not exceed +/-10 ºC temperature differences and the limit established is +/-12.23ºC. Unlike previous configuration, when minimum temperatures were reached, the ends of the gauge length were almost 10ºC warmer than the centre; whereas at maximum cycle temperature, the ends of the gauge length were 10ºC cooler. The reversal in thermal gradients at minimum temperatures turned out to be a good solution to avoid exceeding the established limits.

4.2 Theoretical results

Radial gradients assessment was done by matching a FEM model with experimental results as explained in section 3. As a result, a theoretical thermal transient cycle was obtained which fitted with the experimental TMF cycle.

The test-piece cross-section (quarter of it due to symmetry) was plotted, taken from the centre of the gauge length. Its temperature distribution was similar to that obtained by analytical solutions (Figure 3) with the same elliptical isothermal lines. This is shown in Figure 9.

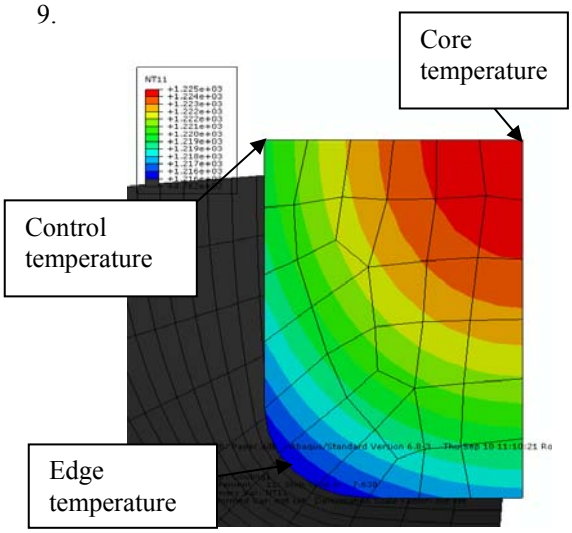

Figure 9. Maximum radial gradients in a TMF cycle

The simulation suggested that maximum radial gradients are around 9.5ºC which is distributed as follows:

a) 5ºC difference between control and core temperature.
b) -4.5 ºC difference between edge and control (Figure 9). Control temperature is the one with whom experimental TMF cycles are controlled

Although TMF standard [1] does not give a limit value for radial gradients, they have to be restricted to avoid premature failure of the test-piece. For this purpose, the static FEM analysis carried out with the temperature distribution file was studied. It was concluded that thermally induced stresses, according to von Mises criteria, may reached up to 30 MPa (lower than 5% of the stress range, $\Delta\sigma$, in a typical TMF test) within the gauge length. Besides, in the FEM thermal analysis, the effect of the grip heating was not added and therefore the assessed stresses were much higher than those in real TMF tests.

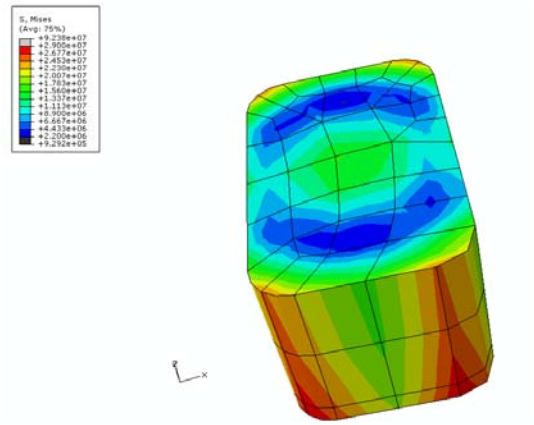

Figure 10. Thermally induced stresses according to von Mises criteria

In Figure 10 stresses caused by the temperature distribution are plotted for a whole cross section. This magnitude is higher at those locations where temperature differences are larger, such as the corners of the test-piece.

If stress tensor main components are analyzed, it may be observed that on the surface tensile stresses appear, whereas at the core the components are mainly compressive. Nevertheless, tensile values are much higher for all the cases and besides it has to be emphasized that in the fatigue phenomena cracks initiate on the surface, where induced tensile stresses are found to be maximum. Consequently the obtained temperature distribution may contribute to the crack initiation and therefore may reduce the life of the test-piece.

As expected, the stress values along the test-piece axis, in other words σ_{33} values, are observed to be most damaging due to the fact that they are originated by the axial gradients (the highest temperature differences). On the other hand, stresses caused by radial gradients, σ_{11} and σ_{22}, are considerably lower (60%). This means that cracks will tend to grow perpendicular to the direction where maximum stresses are observed, longitudinal direction.

5. CONCLUSIONS

i) Executing a non-isothermal fatigue test by Joule effect heating device may cause high axial gradients if test-piece has different area sections.

ii) A method was developed to avoid these gradients which gave excellent result, fulfilling the ASTM standard. For this purpose, heat had to be supplied to the grips.

iii) Although test-piece cross-section is small, radial gradients are produced mainly due to radiation heat exchange which is huge at peak temperature (1223 K in this case) and the high emissivity values (0.85) which increases with temperature and oxidation state.

iv) Coupled thermal-electric model developed in ABAQUS matches with experimental results and gives an excellent solution to those problems whose analytical solution is difficult.

v) Thermally induced stresses were assessed, concluding that tensile stresses prevail over compressive (mainly on the surface of the test-piece) and this may accelerate the crack initiation.

REFERENCES

[1] **ASTM E 2368-04**, "Standard Practised for Strain Controlled Thermomechanical Fatigue Testing". **American Society for Testing and Materials, ASTM, Philadelphia, USA, 2005.**

[2] **Ala-Outinen, Tiina**. "*Fire resistance of austenitic stainless steels Polarit 725 and Polarit 761"* **VTT Tiedotteita -Meddelanden Research Notes 1760. 34 p. + app. 30 p, Finland, 1996.**

[3] **T. Brendel et al**. "Temperature gradients in TMF specimens. Measurement and influence on TMF life". ***International Journal of Fatigue 30 (2008) 234-240.***

ACKNOWLEDGEMENT

Thanks are given to ITP for its financial support and materials; to the Spanish Ministry of Science and Innovation for the financial support (project MAT2008-03735/MAT) and to the Basque Government (project PI09-09).